*Inorg. Chem.* **2004**, *43*, 4751–4760

# Phase Stability in the Systems $AeAl_{2-x}Mg_x$ (Ae = Ca, Sr, Ba): Electron Concentration and Size Controlled Variations on the Laves Phase Structural Theme

**Shahrad Amerioun,[†] Tadahiro Yokosawa,[‡] Sven Lidin,[†] and Ulrich Häussermann*[,†]**

*Department of Inorganic Chemistry and Department of Structural Chemistry, Stockholm University, 10691 Stockholm, Sweden*

Received February 16, 2004

The systems $AeAl_{2-x}Mg_x$ (Ae = Ca, Sr, Ba) display electron concentration induced Laves phase structural changes. However, the complete sequence $MgCu_2 \rightarrow MgNi_2 \rightarrow MgZn_2$ with increasing $x$ (decreasing electron count) is only observed for Ae = Ca. Compounds $SrAl_{2-x}Mg_x$ ($0 < x \leq 2$) and $BaAl_{2-x}Mg_x$ ($x = 0.85$ and 2.0) were synthesized and structurally characterized by X-ray diffraction experiments. For the Sr system the structural sequence $CeCu_2 \rightarrow MgNi_2 \rightarrow MgZn_2$ occurs with increasing Mg content $x$. Thus, larger Sr does not allow the realization of the $MgCu_2$ structure at low $x$. For Ae = Ba a binary compound $BaAl_2$ does not exist, but more Ba-rich $Ba_7Al_{13}$ forms. The reinvestigation of the crystal structure of $Ba_7Al_{13}$ by selected area and convergent beam electron diffraction in a transmission electron microscope revealed a superstructure, which subsequently could be refined from single X-ray diffraction data. The formula unit of the superstructure is $Ba_{21}Al_{40}$ (space group $P31m$, $Z = 1$, $a = 10.568(1)$ Å, $c = 17.205(6)$ Å). In $Ba_{21}Al_{40}$ a size match problem between Ba and Al present in $Ba_7Al_{13}$ is resolved. The structure of $Ba_7Al_{13}$ ($Ba_{21}Al_{40}$) can be considered as a Ba excess variant of the hexagonal $MgNi_2$ Laves phase type structure. An incommensurately modulated variant of the $MgNi_2$ structure is obtained for phases $BaAl_{2-x}Mg_x$ with $x = 0.8$–1. At even higher Mg concentrations a structural change to the proper $MgZn_2$ type structure takes place.

## 1. Introduction

Polar intermetallic compounds bridge charge-balanced Zintl phases and fully delocalized metallic systems.[1−3] This intermediate situation is especially evident in systems $AeE_2$ of heavier alkaline earth metals (Ae = Ca, Sr, Ba) with triels Al, Ga, In (E). Compounds with Ga and In afford structures with polyanionic networks formed by the E component.[4] Three different structure types occur: orthorhombic $CeCu_2$ and hexagonal $CaIn_2$, both with three-dimensional four-connected (3D4C) networks, and the $AlB_2$-type with planar hexagon layers. This is in accord with the Zintl concept: Formally $E^-$, which is isoelectronic to a tetrel element, may form four-connected polyanions with (distorted) tetrahedrally coordinated atoms or three-connected graphitic layers. For systems $AeAl_2$, where the electronegativity difference between Ae and E component is least, a different structural chemistry emerges. Only $SrAl_2$ adopts a structure in agreement with the Zintl concept ($CeCu_2$-type).[5] $CaAl_2$ forms the cubic Laves phase structure $MgCu_2$[6] (Figure 1a), and $BaAl_2$ does not exist at ambient conditions but decomposes into $Ba_7Al_{13}$ and $BaAl_4$.[7] $Ba_7Al_{13}$ (Figure 1e) can be considered as a Ba excess variant of the hexagonal $MgNi_2$ Laves phase structure (Figure 1c).[8]

In the Laves phase $CaAl_2$ the connectivity of the Al network is increased to six, which implies delocalized

* Author to whom correspondence should be addressed. E-mail: ulrich@inorg.su.se.
[†] Department of Inorganic Chemistry.
[‡] Department of Structural Chemistry.

(1) (a) Corbett, J. D. *Angew. Chem., Int. Ed.* **2000**, *39*, 670. (b) Corbett, J. D. *Inorg. Chem.* **2000**, *39*, 5178. (c) Corbett, J. D. In *Chemistry, Structure and Bonding of Zintl Phases and Ions*; Kauzlarich, S., Ed.; VCH: New York, 1996; pp 139−181.
(2) Cordier, G.; Eisenmann, B. In *Chemistry, Structure and Bonding of Zintl Phases and Ions*; Kauzlarich, S., Ed.; VCH: New York, 1996; pp 61−137.
(3) Häussermann, U.; Amerioun, S.; Eriksson, L.; Lee, C.-S.; Miller, G. J. *J. Am. Chem. Soc.* **2002**, *124*, 4371.
(4) Villars, P.; Calvert, L. D. *Pearsons Handbook of Crystallographic Data for Intermetallic Compounds*, 2nd ed.; ASM International: Materials Park, OH, 1991; Desk Edition, 1997.
(5) Nagorsen, G.; Posch, H.; Schäfer, H.; Weiss, A. *Z. Naturforsch.* **1969**, *24b*, 1191.
(6) Nowotny, H.; Wormness, E.; Mohrnheim, A. *Z. Metallkd.* **1940**, *32*, 39.

10.1021/ic0400235 CCC: $27.50 
Published on Web 07/01/2004

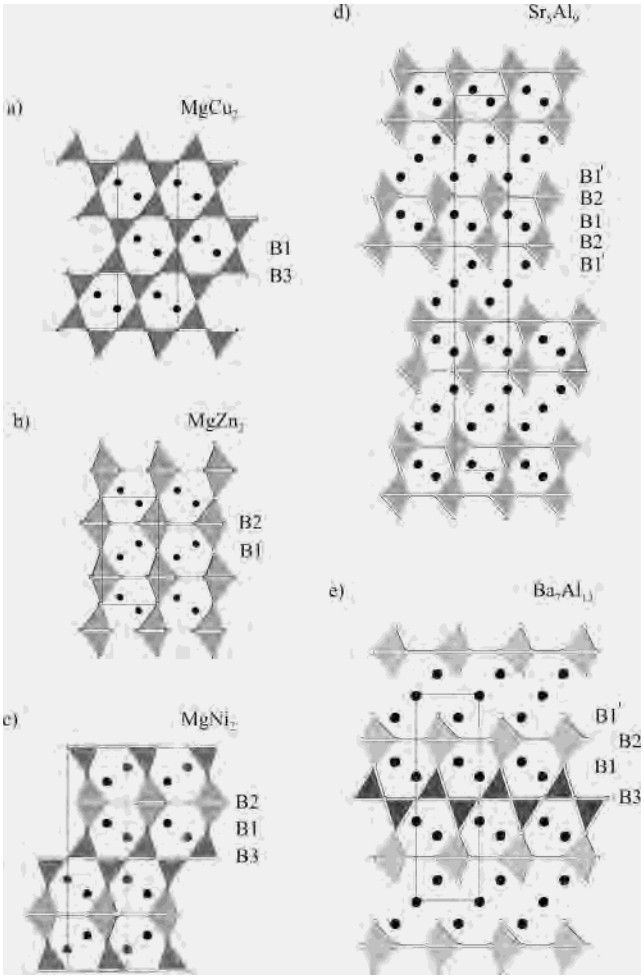


**Figure 1.** Structures of $MgCu_2$ (a), $MgZn_2$ (b), $MgNi_2$ (c), $Sr_5Al_9$ (d), and $Ba_7Al_{13}$ (e). The majority atoms are denoted as B. B2 and B3 represent atoms on Kagome nets, and atoms B1 cap triangles of the Kagome net yielding layers of trigonal bipyramids (with B2) or double layers of tetrahedra (with B3). In the primary Laves phase structures $MgCu_2$, $MgZn_2$, and $MgNi_2$ layers are connected by shared B1 atoms. In cubic $MgCu_2$ B1 and B3 are the same kind of atom. This structure is presented rhombohedrally (with hexagonal axes) for better comparability with the others. In the Ae excess Laves phase structures $Sr_5Al_9$ and $Ba_7Al_{13}$ B1 atom condensed layers are disrupted into separated blocks. B1 atoms at the boundary of such blocks are denoted with primes.

bonding. Generally, Laves phases $AB_2$ occur in three primary structure types, cubic $MgCu_2$ and hexagonal $MgZn_2$ and $MgNi_2$ (Figure 1a−c).[9,10] The structures are intimately related and represent close-packed arrangements of differently sized spheres (topological close-packings). Laves phases appear rather frequently among main group intermetallic $AB_2$ systems upon reduction of the electronegativity difference between the A and B component.[4] Although the Laves phase structures cannot be rationalized by simple electron counting rules, there is a clear relationship between the valence electron concentration (number of valence electrons per atom) and the particular Laves phase structure type that is adopted. This has been revealed in the pseudobinary systems $CaAl_{2-x}Li_x$[11] and $CaAl_{2-x}Mg_x$[12] where with increasing $x$ (decreasing electron concentration) the sequence of Laves phase structures $MgCu_2 \rightarrow MgNi_2 \rightarrow MgZn_2$ is obtained. Further, the formation of Laves phase structures seems to be strongly influenced by the size ratio between the A and B components. The formation of $Ba_7Al_{13}$ ($BaAl_{1.857}$) instead of $BaAl_2$ indicates a size mismatch between Ba and Al. This situation occurs also in the system Sr−Al. Besides charge-balanced $SrAl_2$ (with the $CeCu_2$ structure) there exists as well $Sr_5Al_9$ ($SrAl_{1.8}$), which corresponds to a Sr excess derivate of the $MgZn_2$ Laves phase structure (Figure 1d).[13]

In this work we attempt to rationalize the electron concentration and size controlled formation of Laves phase structures and their Ae excess derivatives in binary $AeAl_2$ and quasibinary $AeAl_{2-x}Mg_x$ systems. In particular, we investigated structural competition in the $AeAl_2$ systems and the phase stability of $Sr_5Al_9$ and $Ba_7Al_{13}$ by first-principles calculations. During this theoretical study we detected inconsistencies in the reported experimental structure of $Ba_7Al_{13}$. We consequently reexamined this structure by single-crystal X-ray diffraction and transmission electron microscopy studies and discovered a superstructure. The refinement of this superstructure changed the formula unit of "$Ba_7Al_{13}$" to $Ba_{21}Al_{40}$ and revealed slight but decisive structural differences, which resolve a subtle size mismatch between Ba and Al still present in the Ae excess Laves phase "$Ba_7Al_{13}$". We further report a comparison of phase stability ranges in $AeAl_{2-x}Mg_x$ where electron concentration controlled Laves phase structural changes occur. Interestingly, in the Ba system—where for compositions $x \approx 1$ a true Laves phase with the $MgNi_2$ structure exists—we observe a situation greatly resembling that for "$Ba_7Al_{13}$". The superstructures of "$Ba_7Al_{13}$" and BaMgAl beautifully demonstrate the structural and compositional flexibility of polar intermetallics to match simultaneously size and electron count requirements for structural stability.[14,15]

## 2. Experimental Section

**2.1. Synthesis.** All materials were prepared from the elements (Sr and Ba pieces (ABCR, 99.9%), Mg granulates (ABCR, 99.9%) and Al ingots (ABCR, 99.9%)) and handled in an Ar filled glovebox ($O_2$ concentration < 2 ppm). For binary $SrMg_2$ and $BaMg_2$ stoichiometric mixtures of the elements were weighed in Ta ampules, which were sealed and placed in fused silica Schlenk tubes under reduced pressure. Reactant mixtures were heated to 850 °C to ensure complete melting followed by rapid quenching to room temperature and subsequent annealing at 550 °C for 5 days. For $SrAl_{2-x}Mg_x$ ($x$ = 0.25, 0.5, 0.75, 1.0, 1.25, 1.5) stoichiometric

(7) (a) Massalski, T. S. *Binary Alloy Phase Diagrams*, 2nd ed.; American Society for Metals: Metals Park, OH, 1990. (b) A high-pressure phase $BaAl_2$ with the $MgCu_2$ structure has been reported by Cordier et al. (Cordier, G.; Czech, E.; Schäfer, H. *Z. Naturforsch.* **1984**, 39b, 421). We note that the lattice parameter of $MgCu_2$-type $BaAl_2$ is abnormally large and that this phase needs reinvestigation.
(8) Fornasini, M. L.; Bruzzone, G. *J. Less-Common Met.* **1975**, *40*, 335.
(9) Hyde, B. G.; Andersson, S. *Inorganic Crystal Structures*; John Wiley & Sons: New York, 1989.
(10) Pearson, W. B. *The Crystal Structure and Physics of Metals and Alloys*; Wiley-Interscience: New York, 1972.
(11) Nesper, R.; Miller, G. J. *J. Alloys Compd.* **1993**, *197*, 109.
(12) Amerioun, S.; Simak, S. I.; Häussermann, U. *Inorg. Chem.* **2003**, *42*, 1467.
(13) Manyako, N. B.; Zarechnyuk, O. S.; Yanson, T. I. *Sov. Phys. Crystallogr.* **1987**, *32*, 196.
(14) (a) Seo, D. K.; Corbett, J. D. *J. Am. Chem. Soc.* **2000**, *122*, 9621. Seo, D. K.; (b) Corbett, J. D. *J. Am. Chem. Soc.* **2001**, *123*, 4512.
(15) Amerioun, S. Doctoral Dissertation, Stockholm University, 2003.

**Table 1.** X-ray Single-Crystal Data Refinement for the Compounds $Ba_7Al_{13}$, $Ba_{21}Al_{40}$, $BaAl_{1.15(3)}Mg_{0.85(3)}$, $BaMg_2$, $SrAl_{1.45(2)}Mg_{0.55(2)}$, $SrAl_{0.96(2)}Mg_{1.04(2)}$, $SrAl_{0.60(7)}Mg_{1.40(7)}$, and $SrMg_2$[a]

| chem formula | $Ba_7Al_{13}$ | $Ba_{21}Al_{40}$ | $BaAl_{1.15(3)}$-$Mg_{0.85(3)}$ | $BaMg_2$ | $SrAl_{1.45(2)}$-$Mg_{0.55(2)}$ | $SrAl_{0.96(2)}$-$Mg_{1.04(2)}$ | $SrAl_{0.60(7)}$-$Mg_{1.40(7)}$ | $SrMg_2$ |
|---|---|---|---|---|---|---|---|---|
| lattice params (Å) | | | | | | | | |
| *a* | 6.0997(3) | 10.5646(4) | 6.2889(16) | 6.6699(9) | 6.0977(14) | 6.1940(3) | 6.3699(8) | 6.4838(3) |
| *c* | 17.269(1) | 17.269(1) | 20.605(8) | 10.602(2) | 19.815(6) | 20.1576(15) | 10.140(2) | 10.4514(8) |
| *V* (Å$^3$) | 556.44(5) | 1669.2(1) | 705.7(4) | 408.46(12) | 638.0(3) | 669.74(6) | 356.33(10) | 380.51(4) |
| space group, *Z* | $P\bar{3}m1$, 1 | $P31m$, 1 | $P6_3/mmc$, 8 | $P6_3/mmc$, 4 | $P6_3/mmc$, 8 | $P6_3/mmc$, 8 | $P6_3/mmc$, 4 | $P6_3/mmc$, 4 |
| formula weight | 1312.12 | 3963.34 | 189.04 | 185.93 | 141.35 | 138.92 | 137.84 | 136.22 |
| $\lambda$ (Å) | 0.71073 | 0.71073 | 0.71073 | 0.71073 | 0.71073 | 0.71073 | 0.71073 | 0.71073 |
| $D_{calc}$ (g cm$^{-1}$) | 3.916 | 3.955 | 3.551 | 3.024 | 2.95 | 2.77 | 2.58 | 2.38 |
| $\mu$ (mm$^{-1}$) | 12.68 | 12.73 | 11.39 | 9.81 | 17.40 | 16.35 | 15.32 | 14.23 |
| R1,[b] wR2[c] | 0.028, 0.075 | 0.024, 0.062 | 0.047, 0.149 | 0.027, 0.060 | 0.017, 0.030 | 0.035, 0.065 | 0.031, 0.133 | 0.012, 0.028 |

[a] The listed compositions of the ternaries were obtained from EDX analyses; all lattice parameters were obtained from Guinier powder pattern; Cu K$\alpha_1$, 23 °C. [b] $R1 = \sum|F_o| - |F_c|/\sum|F_o|$. [c] $wR2 = [\sum[w(F_o^2 - F_c^2)^2]/\sum[w(F_o^2)^2]]^{1/2}$, with $w = 1/[\sigma^2(F_o^2) + (aP)^2 + bP]$ and $P = [2F_c^2 + \mathrm{Max}(F_o^2,0)]/3$.

mixtures of the pure elements were arc-melted. After remelting several times to ensure homogeneity, the samples were annealed in stainless steel ampules for one week at 680 °C and finally quenched to room temperature. Arc-melting caused a loss of Mg (between 15% and 20% of its weight). On the basis of stoichiometric amounts of the starting materials we added an extra 15% Mg to compensate for this loss. $Ba_7Al_{13}$ was prepared by arc-melting samples with the composition $BaAl_2$ (small loss of Al). Further, stoichiometric mixtures of $BaAl_{2-x}Mg_x$ ($x$ = 0.25, 0.5, 0.75, 1.0, 1.25, 1.5) were heated to 720 °C for 24 h followed by rapid quenching to room temperature. The compounds were crushed and pressed to tablets and annealed at 620 °C for 10 days, followed by slow cooling at a rate of 20 K/h to room temperature. Generally, the applied annealing procedures for the synthesis of the ternaries are necessary in order to achieve homogeneous Mg/Al sample compositions. All products obtained were crystalline and exhibited a silvery-gray metallic luster. They were characterized by Guinier powder diagrams (Cu K$\alpha$; Si standard), and their composition was determined with the EDX (energy-disperse X-ray) method in a JEOL 820 scanning electron microscope averaging at least 10 analyses for each sample. For $SrAl_{2-x}Mg_x$, $x$ = 0.25 represents a two-phase region of $CeCu_2$-type $SrAl_2$ and $MgNi_2$-type $SrAl_{2-x}Mg_x$, and $x$ = 1.25 a two-phase region of $MgNi_2$- and $MgZn_2$-type $SrAl_{2-x}Mg_x$. The limiting compositions of the structure types $CeCu_2$, $MgNi_2$, and $MgZn_2$ were determined from these samples. For $BaAl_{2-x}Mg_x$ the situation was found to be different and much more complicated. The main product of sample $x$ = 0.25 was $Ba_7Al_{13-x}Mg_x$. From this sample the limiting composition of $Ba_7Al_{13-x}Mg_x$ was determined ($x$ = 1.3(7)). Samples $x$ = 0.5, 0.75, 1.25, however, resulted in complex mixtures of compounds with different Ba content. This was still the case when annealing the samples for a longer time and/or lowering the annealing temperature. However, the samples $x$ = 1.0 and $x$ = 1.5 were fairly homogeneous and yielded $MgNi_2$-type and $MgZn_2$-type $BaAl_{2-x}Mg_x$, respectively, as main products ($x$ = 1.15(3) and 1.56(8), respectively).

**2.2. Structure Determination. 2.2.1. X-ray Diffraction.** The lattice constants of the investigated systems were obtained from least-squares refinement of measured and indexed lines of the corresponding Guinier powder diffractograms.[16] To ensure proper assignment of the indices the observed lines were compared with the calculated ones using the positional parameters resulting from the structure refinements.[17] Single-crystal intensity data were collected at 293 K from crystals of the samples $SrAl_{2-x}Mg_x$ ($x$ = 0.5/0.55(2), $x$ = 1.0/1.04(2), $x$ = 1.5/1.40(7) (nominal composition/EDX determined compositions)), $SrMg_2$, $Ba_7Al_{13}$, $BaAl_{2-x}Mg_x$ ($x$ = 1.0/0.85(3)), and $BaMg_2$ on a STOE IPDS diffractometer with monochromatic Mo K$\alpha$ radiation ($\lambda$ = 0.71073 Å). All data sets were corrected for Lorentz and polarization effects. Absorption correction was performed by the program X-shape as included in the STOE IPDS software.[18] For structure refinement (full-matrix least-squares on $F^2$) the program SHELX-97 was used.[19] The structures were refined using the atomic position parameters of the $Ba_7Al_{13}$ (space group $P\bar{3}m1$) and $MgNi_2$ and $MgZn_2$ structures (space group $P6_3/mmc$) as starting model. Some details of the single-crystal data collections and refinements are listed in Table 1. Atomic position parameters and selected interatomic distances of the Ba compounds are given in Tables 2−5. Details of the crystal structure investigation of the Sr compounds are given as Supporting Information.

**2.2.2. Electron Microscopy.** A small amount of the $Ba_7Al_{13}$ bulk sample was crushed and dispersed on a carbon thin film on a Cu grid for transmission electron microscopy. Selected-area electron diffraction (SAED) and convergent-beam electron diffraction (CBED) patterns were taken from specimen areas of about 500 and 10 nm in diameter, respectively, at an accelerating voltage of 200 kV using a transmission electron microscope (JEM2000FX). In CBED diffraction patterns are obtained by using a conical electron beam on a specimen area about 10 nm in diameter free from defects and grain and domain boundaries. Instead of the usual diffraction spots, diffraction disks are produced. The point group symmetry of the investigated material can be deduced by inspecting the symmetry appearing in the disks.[20]

**2.3. Electronic Structure Calculations.** Total energy calculations for $AeAl_2$, $Sr_5Al_9$, and $Ba_7Al_{13}$ were performed in the framework of the frozen core all-electron projected augmented wave (PAW) method,[21] as implemented in the program VASP.[22] For each composition $AeAl_2$ we considered the structures $MgCu_2$, $MgZn_2$, and $CeCu_2$. The energy cutoff was set to 400 eV. Exchange and correlation effects were treated by the generalized gradient approximation (GGA), usually referred to as PW91.[23] The integration

(16) Werner, P.-.E. *Ark. Kemi* **1969**, *31*, 513.
(17) Yvon, K.; Jeitschko, W.; Parthé, E. *J. Appl. Crystallogr.* **1977**, *10*, 73.
(18) *IPDS*, version 2.87; Stoe and Cie GmbH: Darmstadt, Germany, 1996. *XSHAPE*: *Crystal Optimisation for Numerical Absorption Correction*; Stoe and Cie GmbH.; Darmstadt, Germany, 1996.
(19) Sheldrick, G. M. *SHELX-97*; University of Göttingen: Göttingen, Germany 1997.
(20) Tanaka, M.; Terauchi, M. *Convergent Beam Electron Diffraction*; JEOL-Maruzen: Tokyo, 1985.
(21) Blöchl, P. E. *Phys. Rev. B* **1994**, *50*, 17953. Kresse, G.; Joubert, J. *Phys. Rev. B* **1999**, *59*, 1758.
(22) Kresse G.; Hafner, J. *Phys. Rev. B* **1993**, *47*, RC558. Kresse, G.; Furthmüller, J. *Phys. Rev. B* **1996**, *54*, 11169.
(23) Perdew, J. P.; Wang Y. *Phys. Rev. B* **1992**, *45*, 13244.

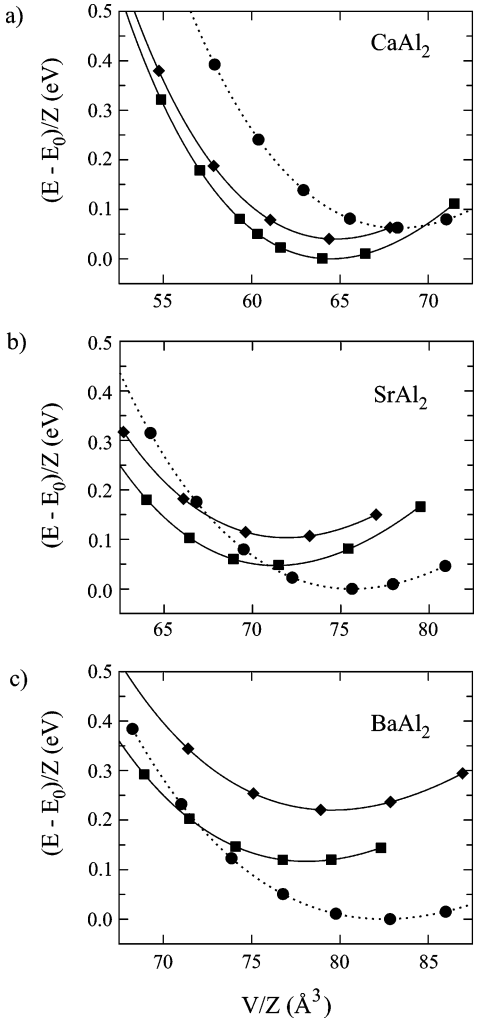


**Figure 2.** Total energy vs volume for the systems $CaAl_2$ (a), $SrAl_2$ (b), and $BaAl_2$ (c) in the structure types $MgCu_2$ (squares), $MgZn_2$ (diamonds), and $CeCu_2$ (circles).

over the Brillouin zone was done on special *k*-points determined according to the Monkhorst−Pack scheme.[24] All necessary convergence tests were performed, and total energies were converged to at least 1 meV/atom. For all systems atomic position parameters and lattice parameters of the considered structures were relaxed for a set of constant volumes until forces had converged to less than 0.01 eV/Å. In a second step we extracted the equilibrium volume $V_{eq}$ and the corresponding energy $E_{eq}$ of each polymorph by fitting the obtained *E* vs *V* values to a Birch−Murnaghan equation of state. A comparison of the relaxed structural parameters with the experimental values is given as Supporting Information.

## 3. Results and Discussion

**3.1. Structural Stability of $AeAl_2$.** We performed first-principles density functional calculations in order to investigate structural competition between the structure types $MgCu_2$, $MgZn_2$, and $CeCu_2$ in the systems $AeAl_2$ and the phase stability of the Laves phase Ae excess compounds $Sr_5Al_9$ and $Ba_7Al_{13}$. Figure 2 summarizes the results of the structural competition study in the $AeAl_2$ systems. For all systems the cubic $MgCu_2$ structure is more favorable than the hexagonal $MgZn_2$ structure. This is expected for main group systems $AB_2$ with eight valence electron per formula unit.[12] For $CaAl_2$ the ground-state $MgCu_2$ structure is lowest in energy, whereas for $SrAl_2$ and $BaAl_2$ the $CeCu_2$ structure is lowest in energy. The destabilization of Laves phase structures with respect to the $CeCu_2$ structure upon increasing the size of Ae is clearly noticeable.

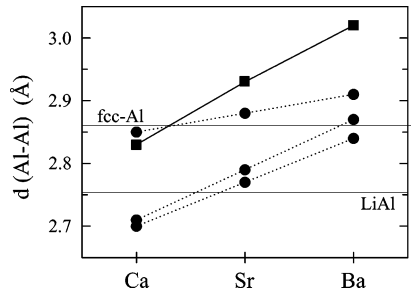


**Figure 3.** Interatomic distances in the computationally relaxed structures $MgCu_2$ (squares, solid line) and $CeCu_2$ (circles, dotted lines) for the systems $AeAl_2$ (Ae = Ca, Sr, Ba).

Figure 3 displays the trend in the distances of $AeAl_2$ in the $MgCu_2$ and $CeCu_2$ structure as obtained from the calculations. The Al−Al network distance in the Laves phase structure increases from 2.83 Å (experimental value 2.84 Å) in $CaAl_2$ to 2.93 Å in $SrAl_2$ to 3.03 Å in $BaAl_2$. In the $CeCu_2$ structure there are three different network distances of which two are very close and the third is distinctly larger. With increasing size of Ae this difference becomes smaller. If the nearest neighbor Al−Al distances in fcc-Al (2.86 Å, 12-coordinated Al) and LiAl (2.76 Å, 4-coordinated $Al^-$) are taken as reference, we can draw the following conclusions. For $MgCu_2$-type $SrAl_2$ the 3D6C Al network becomes too strained and, thus, the $CeCu_2$ structure, with a lower network connectivity (and shorter Al−Al contacts), is realized. This coincides with the findings of Zhang et al. who investigated the system $Ca_{1-x}Sr_xAl_2$.[25] The cubic Laves phase exists for a composition range from $x = 0$ to about $x = 0.8$. For $Ca_{0.2}Sr_{0.8}Al_2$ the Al−Al distance is increased to 2.91 Å. For $SrAl_2$ the $MgCu_2$ and $CeCu_2$ structures are close in energy (cf. Figure 2b), and from our calculations we find a high-pressure transition $CeCu_2$-type → $MgCu_2$-type at 1.8 GPa. This is in agreement with the reported $MgCu_2$-type high-pressure modification of $SrAl_2$, which was obtained at 6 GPa and 1050 °C.[26] Turning to Ae = Ba, the 3D4C network of the $CeCu_2$ structure becomes too strained. The Al−Al distances are in the same range as in 12-coordinated fcc-Al, whereas for $CeCu_2$-type $CaAl_2$ and $SrAl_2$ the two shorter network distances are similar to the Al−Al distance in LiAl. This may explain the nonexistence of $BaAl_2$, i.e. its decomposition into $Ba_7Al_{13}$ (with a Ba excess Laves phase structure) and $BaAl_4$. According to Zhang and Akiba, $CeCu_2$-type $SrAl_2$ tolerates only the substitution of a small amount of Sr by Ba (up to $Sr_{0.92}Ba_{0.08}Al_2$).[27]

In the next step we investigate the phase stability of $Sr_5Al_9$ and $Ba_7Al_{13}$. For that we calculated the energies of formation (formation enthalpies at 0 K) for $Sr_xAl$ ($x = 0.25$, 0.333, 0.357) and $Ba_xAl$ ($x = 0.25$, 0.333, 0.35). These

(24) Monkhorst, H. J.; Pack, J. D. *Phys. Rev. B* **1976**, *13*, 5188.

(25) Zhang, Q. A.; Enoki, H.; Akiba, E. *J. Alloys Compd.* **2001**, *322*, 1257.
(26) Cordier, G.; Czech, E.; Schäfer, H. *Z. Naturforsch.* **1982**, *37b*, 1442.
(27) Zhang, Q. A.; Enoki, H.; Akiba, E. *J. Alloys Compd.* **2002**, *337*, 136.

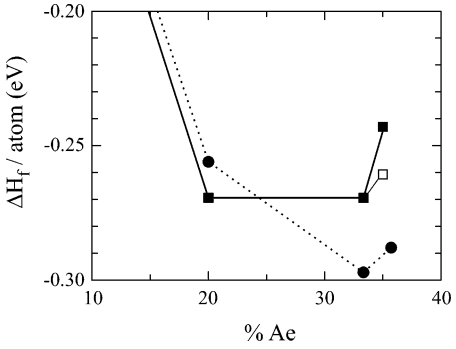


**Figure 4.** Energy of formation ($\Delta H_f(Ae_xAl) = E_{tot}(Ae_xAl) - xE_{tot}(Ae) - E_{tot}(Al)$) for $Ae_xAl$ (Ae = Sr (circles, dotted line) and Ba (squares, solid line)). The following systems were considered: $Ae_{0.25}Al$ ($BaAl_4$ type), $Ae_{0.333}Al$ ($CeCu_2$ type), $Sr_{0.357}Al$ ($Sr_5Al_9$), and $Ba_{0.35}Al$ ($Ba_7Al_{13}$, the open symbol marks the location of $\Delta H_f$ for obtaining zero energy in the decomposition reaction $15BaAl_2$ ($CeCu_2$) = $2Ba_7Al_{13}$ + $BaAl_4$).

formation energies are assembled in Figure 4. Now we consider the energies for the decomposition reactions

$$11SrAl_2\ (CeCu_2) = 2Sr_5Al_9 + SrAl_4 \qquad (1)$$

and

$$15BaAl_2\ (CeCu_2) = 2Ba_7Al_{13} + BaAl_4 \qquad (2)$$

Surprisingly, we find that both reaction energies are positive: 0.455 eV (0.04 eV/$Z$ = 3.87 kJ/mol $SrAl_2$) for eq 1 and 0.726 eV (0.048 eV/$Z$ = 4.65 kJ/mol $BaAl_2$) for eq 2. This means that both compounds, $SrAl_2$ and $BaAl_2$, would be stable with respect to the specified decomposition reaction. For $BaAl_2$ this is in contradiction with the phase diagram.[7] A negative energy value for reaction 2 would require a substantial stabilization of $Ba_7Al_{13}$ by about 10% (indicated in Figure 4). The inspection of the relaxed structural parameters of $Ba_7Al_{13}$ reveals large discrepancies to the experimental values. This is suspicious because for the other investigated binary aluminides (i.e. $SrAl_4$, $BaAl_4$, $CaAl_2$, $SrAl_2$, $Sr_5Al_9$) the agreement between computationally obtained and experimental structural parameters is excellent (cf. Supporting Information). In the original crystal structure refinement by Fornasini and Bruzzone one unreasonably large isotropic thermal parameter (for the position B3) was obtained.[8] This was also noticed recently by Lee and Miller.[28]

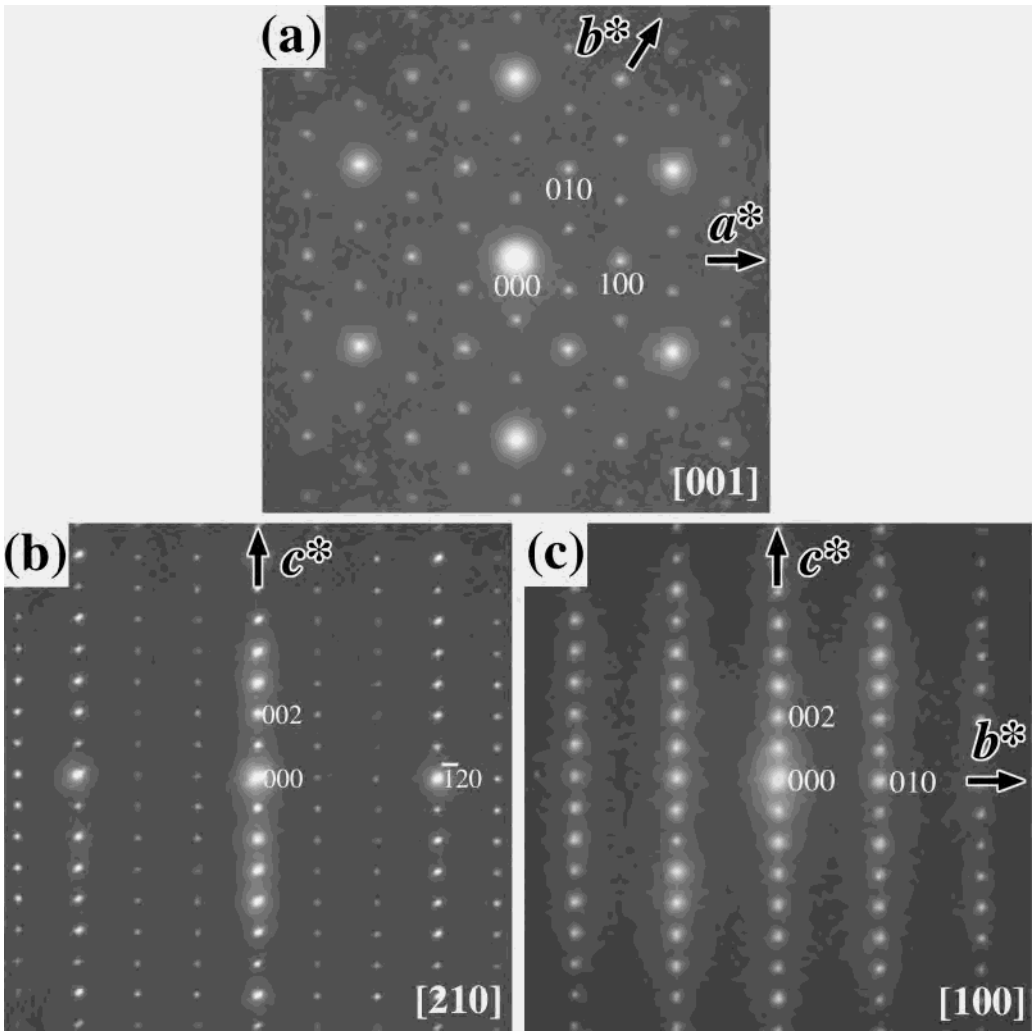


**Figure 5.** [001] (a), [210] (b), and [100] (c) SAED patterns of $Ba_7Al_{13}$. $a^*$ and $b^*$ correspond to the reciprocal lattice vectors of the basis lattice of $Ba_7Al_{13}$. Superlattice reflection spots are clearly recognized in the [001] and [210] directions. The SAED patterns unambiguously reveal a perfectly ordered $\sqrt{3} \times \sqrt{3} \times 1$ superstructure in $Ba_7Al_{13}$.

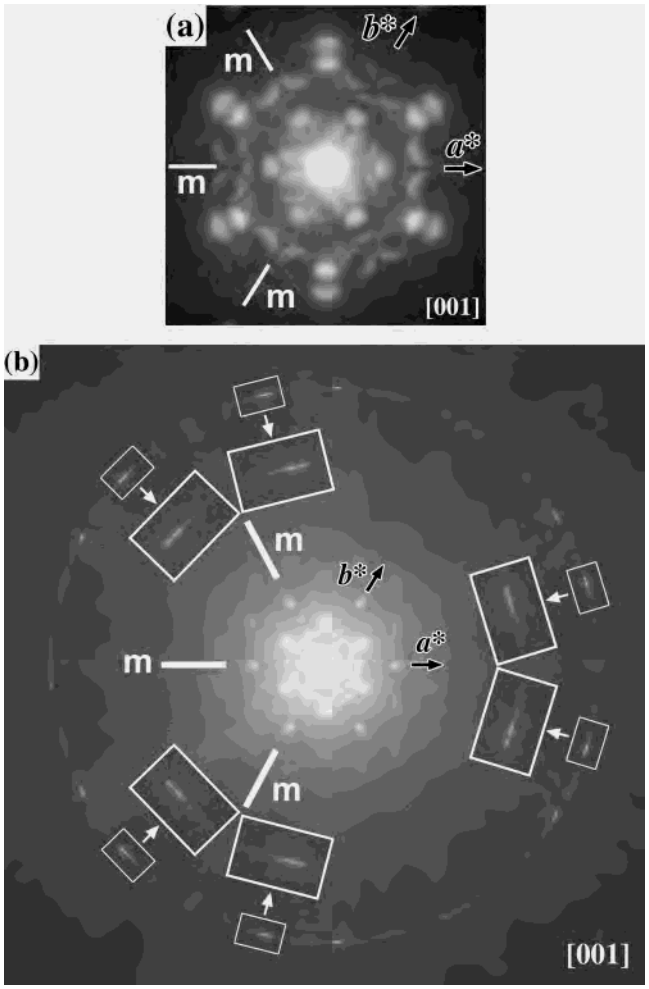


**Figure 6.** (a) [001] CBED pattern of $Ba_7Al_{13}$. The intensity distribution of the superlattice reflection disks around the center has the symmetry 3*m*. (b) [001] CBED pattern of $Ba_7Al_{13}$ including first-order Laue-zone (FOLZ) reflections shows that also the total (three-dimensional) symmetry is 3*m*. Thus, the only possible point group for the superstructure of $Ba_7Al_{13}$ is 3*m*.

**3.2. Superstructure of $Ba_7Al_{13}$.** We prepared $Ba_7Al_{13}$ in quantitative yields from arc-melting samples with the composition $BaAl_2$ and reinvestigated the crystal structure of $Ba_7Al_{13}$. The refinement of the X-ray single-crystal diffraction data using the structural model of Fornasini and Bruzzone (space group $P\bar{3}m1$) yielded very satisfactory residuals (cf. Table 1). However, the thermal displacement parameters at the B1 and especially B3 sites (cf. Figure 1e) were found highly anisotropic (Figure 7a). These positions define a Kagome net (B3) in which the triangles are capped alternately from above and below (B1) to yield a double layer of Al tetrahedra. The distance B1−B3 is 3.38 Å, which would correspond to an extremely strained Al−Al contact. This strain is introduced by the large Ba atoms and, apparently, the formation of the Ae excess Laves phase structure $Ba_7Al_{13}$ could not completely remove the size mismatch between Ba and Al. In the computationally relaxed structure this strain is somewhat released and the B1−B3 distance is reduced to 3.18 Å.

(28) Lee, C.-S.; Miller, G. J. *J. Solid State Chem.* **2003**, *170*, 94.

**Table 2.** Atomic Position Parameters, Site Occupancies, and Isotropic Thermal Parameters (Å$^2$) for $Ba_7Al_{13}$ and $Ba_{21}Al_{40}$

| | Wyckoff | *x* | *y* | *z* | SOF | $U_{eq}$[a] |
|---|---|---|---|---|---|---|
| | | | $Ba_7Al_{13}$ | | | |
| Ba1 | 1a | 0 | 0 | 0 | 1 Ba | 0.032(1) |
| Ba2 | 2c | 0 | 0 | 0.3922(1) | 1 Ba | 0.022(1) |
| Ba3 | 2d | 1/3 | 2/3 | 0.8940(1) | 1 Ba | 0.019(1) |
| Ba4 | 2d | 1/3 | 2/3 | 0.6791(1) | 1 Ba | 0.019(1) |
| B1 | 2d | 1/3 | 2/3 | 0.3332(5) | 1 Al | 0.042(2) |
| B1′ | 2d | 1/3 | 2/3 | 0.0973(3) | 1 Al | 0.020(1) |
| B2 | 6i | 0.1564(3) | 0.8346(3) | 0.2116(2) | 1 Al | 0.025(1) |
| B3 | 3f | 1/2 | 0 | 1/2 | 1 Al | 0.169(7) |
| | | | $Ba_{21}Al_{40}$ | | | |
| Ba11 | 3c | 0.3295(1) | 0 | 0.0006(1) | 1 Ba | 0.021(1) |
| Ba21 | 3c | 0.3228(1) | 0 | 0.6070(1) | 1 Ba | 0.010(1) |
| Ba22 | 3c | 0 | 0.3321(1) | 0.3913(6) | 1 Ba | 0.010(1) |
| Ba31 | 3c | 0.6650(1) | 0 | 0.8932(1) | 1 Ba | 0.010(1) |
| Ba32 | 2b | 2/3 | 1/3 | 0.1048(1) | 1 Ba | 0.010(1) |
| Ba33 | 1a | 0 | 0 | 0.1066(1) | 1 Ba | 0.010(1) |
| Ba41 | 3c | 0.6706(1) | 0 | 0.6792(4) | 1 Ba | 0.010(1) |
| Ba42 | 2b | 2/3 | 1/3 | 0.3200(1) | 1 Ba | 0.010(1) |
| Ba43 | 1a | 0 | 0 | 0.3231(1) | 1 Ba | 0.010(1) |
| B1a | 1a | 0 | 0 | 0.6920(5) | 1 Al | 0.016(1) |
| B1b | 2b | 2/3 | 1/3 | 0.6532(3) | 1 Al | 0.014(1) |
| B1c | 3c | 0.3309(3) | 0.3309(3) | 0.3307(4) | 1 Al | 0.015(1) |
| B1′a | 1a | 0 | 0 | 0.9007(5) | 1 Al | 0.012(1) |
| B1′b | 2b | 2/3 | 1/3 | 0.9036(3) | 1 Al | 0.011(1) |
| B1′c | 3c | 0.3342(3) | 0.3342(3) | 0.0976(3) | 1 Al | 0.010(1) |
| B2a | 3c | 0.1942(4) | 0 | 0.7940(3) | 1 Al | 0.013(1) |
| B2b | 6d | 0.8363(4) | 0.3363(3) | 0.7853(2) | 1 Al | 0.012(1) |
| B2c | 6d | 0.1551(4) | 0.3328(3) | 0.2112(2) | 1 Al | 0.011(1) |
| B2d | 3c | 0.4892(4) | 0 | 0.2117(2) | 1 Al | 0.010(1) |
| B3a | 1a | 0 | 0 | 0.5341(4) | 1 Al | 0.021(1) |
| B3b | 6d | 0.8168(3) | 0.4803(3) | 0.5086(2) | 1 Al | 0.019(1) |
| B3c | 3c | 0 | 0.7591(4) | 0.4793(2) | 1 Al | 0.019(1) |

[a] $U_{eq}$ is defined as one-third of the trace of the orthogonalized $\mathbf{U}_{ij}$ tensor.

SAED patterns obtained from transmission electron microscopy investigations revealed clearly a $\sqrt{3} \times \sqrt{3} \times 1$ superstructure in trigonal $Ba_7Al_{13}$ (Figure 5). The unit cells of the basis structure and superstructure are mutually rotated by 30°. According to the CBED patterns (Figure 6) the trigonal symmetry of the basis structure is retained in the superstructure; the only possible point group symmetry is 3*m*. The superstructure reflections are also detectable by X-ray diffraction on large single crystals. A suitable crystal could be selected, and intensity data was collected using long exposure times.

To solve the superstructure the basis structure was expanded to the $\sqrt{3} \times \sqrt{3} \times 1$ supercell and the symmetry changed to $P\bar{3}1m$ accordingly. As expected, this did not solve the problem of unphysically large displacement parameters. The refinement converged to a rather high residual value, $R \approx 15\%$, and it was noted that the strongest anisotropic effect was located at Wyckoff position 3f, a site with 2/*m* symmetry. The rotation dyad and the inversion center both forbid the displacement of the atom perpendicular to the dyad direction, and hence the only viable alternative for a maximal subgroup was *P*31*m*. Displacing the most anisotropic atom away from the inversion center and lowering the symmetry led to a dramatic decrease of the thermal parameters. A full refinement of all positional and thermal parameters did however not reduce the *R*-value beyond 11%. Large residual electron densities were located at the Ba positions, most notably at those located on the rotation triad. A closer inspection of this residual electron density revealed trefoil-

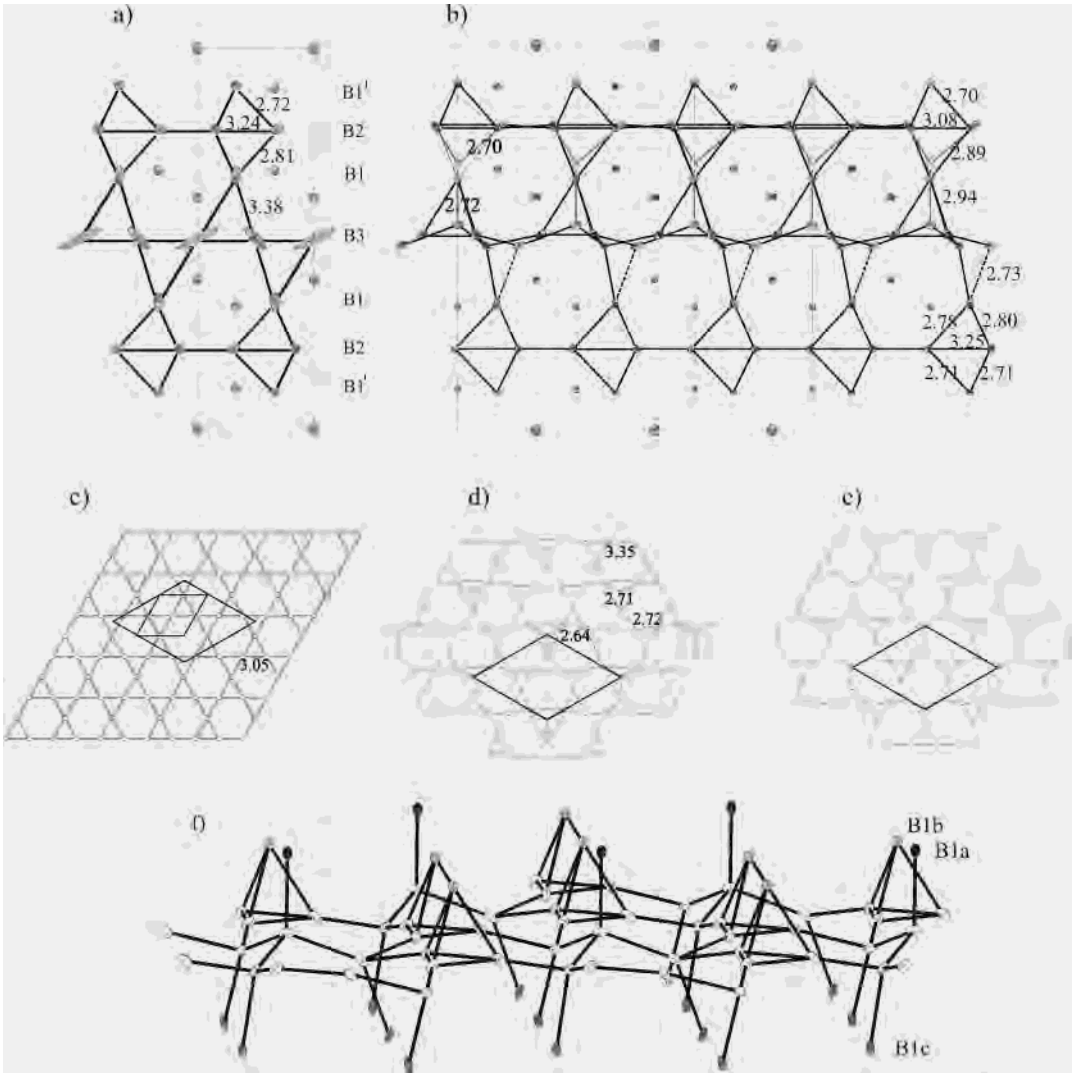


**Figure 7.** Crystal structures of "$Ba_7Al_{13}$" (a) and $Ba_{21}Al_{40}$ (b). The ellipsoid size corresponds to a 50% probability. (c) The Kagome net formed by B3 atoms in "$Ba_7Al_{13}$". The unit cells of $Ba_7Al_{13}$ and $Ba_{21}Al_{40}$ are indicated. (d) The stuffed Kagome net occurring in $Ba_{21}Al_{40}$. Stuffing takes place at the center of the triangles located at the unit cell vertices. (e) The real connectivity in the stuffed Kagome net of $Ba_{21}Al_{40}$. This net consists of elongated octagons and triangles in a ratio 3:2. (f) A perspective view of the stuffed Kagome net of $Ba_{21}Al_{40}$ along [210] illustrating its corrugation and the connectivity of the B3-type atoms to B1-type atoms in the surrounding layers of trigonal bipyramids.

like electron density indicative of a violation of the rotation triad. This may be caused either by a true breaking of symmetry or by an unfortunate choice of origin. Since the CBED patterns give no indication of lower symmetry, an origin shift $-(1/3,0,0)$ was performed, which led to an immediate improvement in *R*-value. After the introduction of an extra Al position indicated by a residual electron density maximum without short contacts to neighboring atoms, the refinement converged at an *R*-value below 3% (cf. Table 1). The final structure model exhibits an additional Al atom in the B3 atom Kagome net (formula unit $Ba_{21}Al_{40}$) and yields reasonable Al−Al distances as well as satisfactory thermal displacement parameters. It is shown in Figure 7b in comparison with the refined basis structure "$Ba_7Al_{13}$" (Figure 7a). Atomic position parameters and important interatomic distances of "$Ba_7Al_{13}$" and $Ba_{21}Al_{40}$ are comparatively presented in Tables 2 and 3.

The most conspicuous difference between "$Ba_7Al_{13}$" and $Ba_{21}Al_{40}$ is the stuffing and corrugation of the B3 atom Kagome net in the latter (Figures 7c−f). The stuffing atom (B3a on the site 1a) actually changes the Kagome net drastically. Formally, this atom enters the centers of $^1/_6$ of the triangles present in the original Kagome net (Figure 7c,d). However, as a consequence of the stuffing a completely different net (Figure 7e) consisting of (elongated) octagons and triangles in a ratio 3:2 is created (written as $(38^2)_6(8^3)_4$ according to the Schläfli nomenclature[29]). The connectivity of the nodes in this net is strictly three (compared to four in the Kagome net), and the corresponding distances are in a narrow range between 2.64 and 2.72 Å (the next largest distance appears at 3.35 Å). For comparison, the interatomic distance in the four-connected Kagome net of "$Ba_7Al_{13}$" is 3.05 Å. The corrugation of the $(38^2)_6(8^3)_4$ net ensures reasonable Al−Al distances to the B1-type atoms of the trigonal bipyramids (Figure 7f). There are two types of B1−B3 connections: B1a and B1c atoms are connected to one B3 atom at distances of 2.73 and 2.74 Å, respectively, whereas B1b atoms are connected to three B3 atoms at a distance of

(29) The Schläfli symbols denote the types and numbers of polygons around a net point ($n^m = m$ *n*-gons.[10]

**Table 3.** Important Interatomic Distances (Å) in $Ba_7Al_{13}$ and $Ba_{21}Al_{40}$

$Ba_7Al_{13}$

| Ba−B distances | | | | B−B distances | | | |
|---|---|---|---|---|---|---|---|
| Ba1−B1′ | 3.902(2) × 6 | Ba3−B1′ | 3.512(5) | B1−B2 | 2.812(7) × 3 | B2−B1′ | 2.718(4) |
| | | Ba3− B1′ | 3.525(1) × 3 | B1−B3 | 3.376(7) × 3 | B2−B1 | 2.812(7) |
| Ba2−B2 | 3.529(3) × 3 | Ba3−B2 | 3.555(1) × 6 | | | B2−B2 | 2.861(6) × 2 |
| Ba2−B3 | 3.573(1) × 6 | | | B1′−B2 | 2.718(4) × 3 | B2−B2 | 3.238(6) × 2 |
| Ba2−B1 | 3.666(2) × 3 | Ba4−B1 | 3.528(1) × 3 | | | | |
| | | Ba4−B3 | 3.559(1) × 3 | | | B3−B3 | 3.050(1) × 4 |
| | | Ba4−B2 | 3.590(2) × 6 | | | B3−B1 | 3.376(7) × 2 |

$Ba_{21}Al_{40}$

| Ba−B distances | | | | B−B distances | | | |
|---|---|---|---|---|---|---|---|
| Ba11− | | Ba32− | | B1a− | | B2b− | |
| B2a | 3.844(5) | B1′b | 3.474(6) | B2a | 2.703(7) × 3 | B1′b | 2.708(6) |
| B1′a | 3.885(4) | B1′c | 3.520(2) × 3 | B3a | 2.727(10) | B2a | 2.804(6) |
| B1′c | 3.886(3) × 2 | B2d | 3.567(2) × 3 | | | B1b | 2.892(6) |
| B1′b | 3.918(3) × 2 | B2c | 3.567(3) × 3 | B1b− | | B2b | 2.995(7) |
| B2c | 3.982(4) | | | B2b | 2.892(6) × 3 | B2b | 3.078(7) × 2 |
| | | Ba33− | | B3b | 2.948(6) × 3 | | |
| Ba21− | | B1′c | 3.534(3) × 3 | | | B2c− | |
| B2a | 3.504(5) | B2c | 3.542(3) × 6 | B1c− | | B1′c | 2.720(5) |
| B3b | 3.529(3) × 2 | B1′a | 3.557(8) | B3c | 2.736(7) | B1c | 2.783(6) |
| B3b | 3.552(3) × 2 | | | B2c | 2.783(6) × 2 | B2c | 2.840(7) |
| B2b | 3.569(4) × 2 | Ba41− | | B2d | 2.800 (6) | B2d | 2.850(6) |
| B3a | 3.635(3) | B1a | 3.487(1) | B3b | 3.647(6) × 2 | | |
| B1b | 3.667(1) × 2 | B3b | 3.545(4) × 2 | | | B2d− | |
| | | B2b | 3.566(3) × 2 | B1′a− | | B1′c | 2.713(6) |
| Ba22− | | B1b | 3.571(1) × 2 | B2a | 2.757(7) × 3 | B1c | 2.800(6) |
| B3c | 3.488(2) × 2 | B3c | 3.576(4) | | | B2c | 2.850(6) × 2 |
| B2c | 3.514(3) × 2 | B2b | 3.581(3) × 2 | B1′b− | | | |
| B2d | 3.518(4) | B2a | 3.621(3) × 2 | B2b | 2.708(6) × 3 | B3a− | |
| B3b | 3.651(3) × 2 | | | | | B3c | 2.715(5) × 3 |
| B1c | 3.655(3) × 2 | Ba42− | | B1′c− | | B1a | 2.727(10) |
| B3b | 3.691(3) × 2 | B1c | 3.540(2) × 3 | B2d | 2.713(6) | | |
| | | B2d | 3.580(2) × 3 | B2c | 2.720(5) × 2 | B3b− | |
| Ba31− | | B2c | 3.588(3) × 3 | | | B3c | 2.642(4) |
| B1′b | 3.518(1) × 2 | B3b | 3.616(4) × 3 | B2a− | | B3b | 2.720(6) × 2 |
| B2a | 3.522(2) × 2 | | | B1a | 2.703(7) | B1b | 2.948(6) |
| B1′c | 3.531(5) | Ba43− | | B1′a | 2.757(7) | | |
| B2b | 3.538(3) × 2 | B1c | 3.498(3) × 3 | B2b | 2.804(6) × 2 | B3c− | |
| B1′a | 3.541(1) | B2c | 3.608(3) × 6 | | | B3b | 2.642(4) × 2 |
| B2b | 3.597(3) × 2 | B3a | 3.644(7) | | | B3a | 2.715(5) |
| | | | | | | B1c | 2.736(7) |

2.95 Å. For comparison, in "$Ba_7Al_{13}$" all B1 atoms are connected to three B3 atoms at a distance of 3.38 Å. Further, in $Ba_{21}Al_{40}$ all B3-type are clearly four-connected. Interestingly, a closely related situation is encountered in newly discovered $Ba_{14}Al_{22+x}Zn_{5-x}$.[28] This compound has a monoclinic (pseudo-orthorhombic) structure with a unit cell close to a $\sqrt{3}a \times b \times 2c$ supercell of "$Ba_7Al_{13}$". There a different stuffing of the B3 atom Kagome net is realized, which subsequently also appears corrugated to yield reasonable B1−B3 distances.

**3.3. The Systems $AeAl_{2-x}Mg_x$.** The system $CaAl_{2-x}Mg_x$ displays the sequence of Laves phase structures $MgCu_2 \rightarrow MgNi_2 \rightarrow MgZn_2$ with increasing Mg concentration $x$. We found that these structural changes are induced by the valence electron concentration.[12] The origin of this structural trend upon decreasing the electron concentration may be explained by the method of moments: When going from the $MgCu_2$ to the $MgZn_2$ structure the four-membered ring concentration (and thus the fourth moment) in the B atom network is successively increased, which stabilizes a structure at a lower band filling. Recently, Zhang and Akiba reported on phase relations in $SrAl_{2-x}Mg_x$.[30] However, in this work the homogeneity ranges of the different phases were not clearly defined, because sample compositions were not explicitly analyzed. Here we present a comparison of the structural changes in the systems $AeAl_{2-x}Mg_x$, which is based on our own findings on $SrAl_{2-x}Mg_x$ and also includes hitherto not investigated $BaAl_{2-x}Mg_x$.

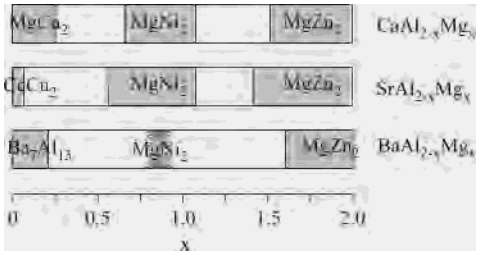


**Figure 8.** Homogeneity ranges in $AeAl_{2-x}Mg_x$. White areas correspond to two-phase regions. For $MgNi_2$-type $BaAl_{2-x}Mg_x$ the homogeneity range could not be determined.

The homogeneity ranges of the different phases occurring in $AeAl_{2-x}Mg_x$ are summarized in Figure 8. For $SrAl_{2-x}Mg_x$ the structural sequence $CeCu_2 \rightarrow MgNi_2 \rightarrow MgZn_2$ is observed. $CeCu_2$-type $SrAl_2$ tolerates only the exchange of

(30) Zhang, Q. A.; Akiba, E. *J. Alloys Compd.* **2003**, *360*, 143.

**Table 4.** Atomic Position Parameters, Site Occupancies, and Isotropic Thermal Parameters (Å$^2$) for $BaAl_{1.15(3)}Mg_{0.85(3)}$ and $BaMg_2$

| | Wyckoff | *x* | *y* | *z* | SOF | $U_{eq}$[a] |
|---|---|---|---|---|---|---|
| | | | $BaAl_{1.15(3)}Mg_{0.85(3)}$ | | | |
| Ba1 | 4e | 0 | 0 | 0.0946(1) | 1 Ba | 0.034(1) |
| Ba2 | 4f | 1/3 | 2/3 | 0.3444(1) | 1 Ba | 0.022(1) |
| B1 | 4f | 1/3 | 2/3 | 0.1442(7) | 1 Mg/Al | 0.021(1) |
| B2 | 6h | 0.1602(7) | 0.3204(7) | 1/4 | 1 Mg/Al | 0.049(3) |
| B3 | 6g | 0 | 1/2 | 1/2 | 1 Mg/Al | 0.137(10) |
| | | | $BaMg_2$ | | | |
| Ba | 4f | 1/3 | 2/3 | 0.0572(1) | 1 Ba | 0.022(1) |
| B1 | 2a | 0 | 0 | 0 | 1 Mg | 0.021(1) |
| B2 | 6h | 0.8376(4) | 0.6752(4) | 1/4 | 1 Mg | 0.023(1) |

[a] $U_{eq}$ is defined as one-third of the trace of the orthogonalized $\mathbf{U}_{ij}$ tensor.

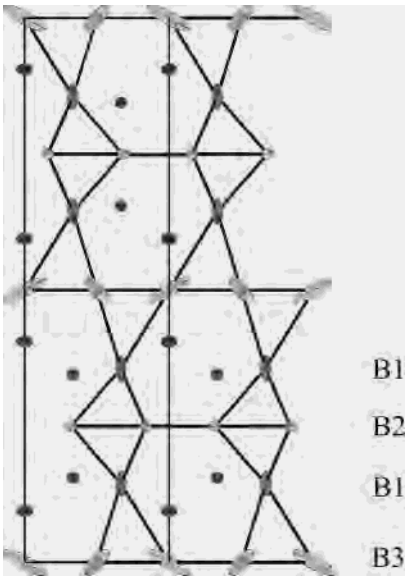


**Figure 9.** The (basis) structure of $BaAl_{1.15}Mg_{0.85}$. The ellipsoid size corresponds to a 50% probability.

a small amount of Al by Mg. The limiting composition *x* is about 0.1. The homogeneity range of the $MgNi_2$-type phase is $0.55(2) < x < 1.04(2)$ and that of the $MgZn_2$-type phase $1.40(7) < x \leq 2.0$. Crystallographic details are given as Supporting Information. The regions between stability ranges correspond to two-phase regions. The $MgNi_2$ and $MgZn_2$ phases have very similar homogeneity ranges in $CaAl_{2-x}Mg_x$ and $SrAl_{2-x}Mg_x$. Generally, the exchange of Al for Mg increases interatomic distances in the B atom networks. Thus, upon incorporation of Mg in the Al framework of $SrAl_2$ the size mismatch between Sr and Al prohibiting the formation of $MgCu_2$ at ambient conditions is released and a Laves phase structure is formed at a certain concentration of Mg. This is the $MgNi_2$ structure, because the incorporation of Mg simultaneously implies a reduction of the electron concentration. (However, the incorporation of Mg also decreases the electronegativity difference between the A and B components, which generally favors the formation of Laves phase structures in main group $AB_2$ intermetallic systems).

Concerning $BaAl_{2-x}Mg_x$, binary $BaAl_2$ does not exist, but "$Ba_7Al_{13}$" ($Ba_{21}Al_{40}$) with a Ba excess Laves phase structure, which was discussed in detail before, forms. A small amount of Mg (about 6 atom %) can be incorporated in "$Ba_7Al_{13}$", and it is not yet clear if this substitution affects its superstructure (i.e. the structure of $Ba_{21}Al_{40}$). For *x* around

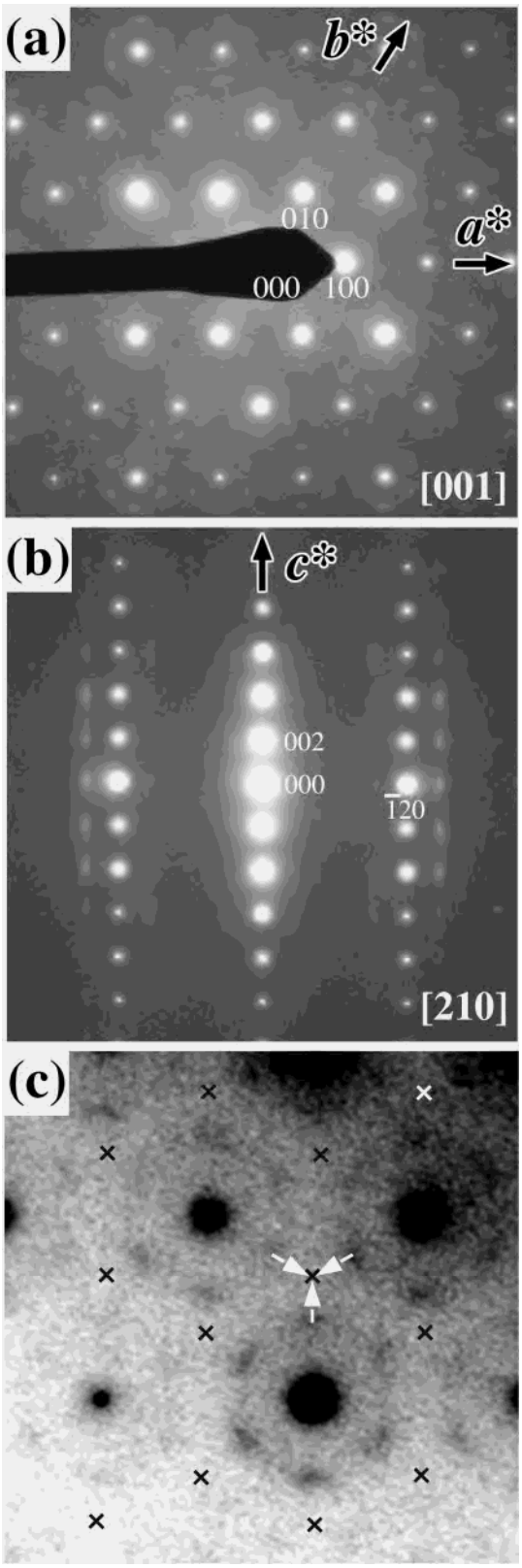


**Figure 10.** [001] (a) and [210] (b) SAED patterns of $BaAl_{1.15}Mg_{0.85}$ (BaAlMg). Diffuse superlattice reflections are recognized in both directions. (c) Distribution of superlattice reflections of "$Ba_7Al_{13}$" (crosses) and BaAlMg in the [001] direction. The "$Ba_7Al_{13}$" reciprocal lattice is created when merging three BaAlMg superlattice reflections into one, as indicated by the white arrows.

1.0 $BaAl_{2-x}Mg_x$ adopts the $MgNi_2$ Laves phase structure (Tables 4 and 5), which is in agreement with the other

**Table 5.** Important Interatomic Distances (Å) in $BaMg_2$ and $BaAl_{1.15(3)}Mg_{0.85(3)}$

$BaAl_{1.15(3)}Mg_{0.85(3)}$

| Ba−B distances | | B−B distances | |
|---|---|---|---|
| Ba1−B2 | 3.647(4) × 3 | B1−B2 | 2.88(1) × 3 |
| Ba1−B3 | 3.699(1) × 6 | B1−B3 | 3.48(1) × 3 |
| Ba1−B1 | 3.772(4) × 3 | | |
| | | B2−B1 | 2.88(1) × 2 |
| Ba2−B1 | 3.638(1) × 3 | B2−B2 | 3.02(1) × 2 |
| Ba2−B3 | 3.684(2) × 3 | B2−B2 | 3.27(1) × 2 |
| Ba2−B2 | 3.699(1) × 6 | | |
| | | B3−B3 | 3.144(1) × 4 |
| | | B3−B1 | 3.48(1) × 2 |

$BaMg_2$

| Ba−B distances | | B−B distances | |
|---|---|---|---|
| Ba1−B2 | 3.809(2) × 3 | B1−B2 | 3.247(2) × 6 |
| Ba1−B1 | 3.898(1) × 3 | | |
| Ba1−B2 | 3.912(1) × 6 | B2−B1 | 3.247(2) × 2 |
| | | B2−B2 | 3.249(7) × 2 |
| | | B2−B2 | 3.421(7) × 2 |

systems. For this phase a definite homogeneity range could not be established. At higher Mg concentrations the $MgNi_2$-type phase is succeeded by $MgZn_2$-type $BaAl_{2-x}Mg_x$, which has its stability interval in the range $1.5 < x \leq 2.0$. Similarly as in the system $SrAl_{2-x}Mg_x$ the incorporation of Mg raises the size mismatch and a proper Laves phase $AB_2$ succeeds the Ae excess variant "$Ba_7Al_{13}$" at a certain Mg content. Interestingly, analogous to "$Ba_7Al_{13}$" in $MgNi_2$-type BaAlMg the distance between B1 and B3 atoms within the double layer of tetrahedra is very large, 3.48 Å. For comparison, the B−B distances in binary $MgZn_2$-type $BaMg_2$ are 3.25 and 3.42 Å (Tables 4 and 5). The thermal displacement parameters at the B1 and B3 sites are highly anisotropic (Figure 9) and greatly resemble those found for the basis structure of "$Ba_7Al_{13}$" (cf. Figure 7a). Single-crystal X-ray diffraction experiments gave no evidence of a superstructure formation. However, we suspect that BaAlMg with a proper Laves phase structure suffers the same size mismatch as "$Ba_7Al_{13}$", and the B3 atom arrangement in BaAlMg is expected to be similar to that in $Ba_{21}Al_{40}$. Indeed, SAED experiments revealed rather weak superstructure reflections in the $a^*b^*$ plane of the $MgNi_2$-type basis lattice (Figure 10a,b). These reflections form separated hexagons around each basis structure reflection and are incommensurate with the basis lattice. They have a large diffuse contribution which extends into the $c^*$ direction (Figure 10b). The relationship to the $Ba_{21}Al_{40}$ reciprocal lattice (cf. Figure 5a) is easily recognized. It appears when three BaAlMg superstructure reflections from three different hexagons are merged into one reflection (Figure 10c). However, as manifested by the incommensurate and diffuse nature of the reflections the superstructure of BaAlMg is more complex than that of "$Ba_7Al_{13}$", and its complete characterization has not been possible for the time being.

## 4. Conclusions

Polar intermetallics $AeE_2$ (Ae = Ca, Sr, Ba; E = Al, Ga, In) display a variety of crystal structures. Gallides and indides crystallize with structures in accord with the Zintl concept and may be considered as charge-balanced. Aluminides show a strong tendency to form Laves phase structures, which, however, is hidden by a size mismatch for Ae = Sr and Ba. This size mismatch is expressed in the formation of compounds with a composition close to $AeAl_2$, i.e. $Sr_5Al_9$ ($Sr_5Al_{1.8}$) and $Ba_7Al_{13}$ ($BaAl_{1.857}$). The structures of these compounds can be considered as Ae excess derivates of Laves phase structures. Excess Ae breaks up the Laves phase 3D network of the Al atoms into slabs. The size mismatch between Ae (Sr, Ba) and Al can be resolved by substituting Al for larger Mg. At a certain concentration of Mg, proper Laves phases (with 3D networks) occur in the ternay systems $AeAl_{2-x}Mg_x$ (Ae = Sr, Ba). The incorporation of Mg reduces at the same time the electron count, which induces Laves phase structural changes. Although Laves phases cannot be rationalized by simple electron counting rules, there is a clear relationship between the valence electron concentration and the particular Laves phase structure that is adopted. The general structural trend in $AeAl_{2-x}Mg_x$ is the sequence $MgCu_2 \rightarrow MgNi_2 \rightarrow MgZn_2$ with increasing $x$ (decreasing electron count). The complete sequence, however, is observed only for Ae = Ca.[12]

The reinvestigation of the crystal structure of the Ae excess Laves phase $Ba_7Al_{13}$ revealed a $\sqrt{3} \times \sqrt{3} \times 1$ superstructure. The refinement of this superstructure changed the formula unit to $Ba_{21}Al_{40}$. This compositional change together with slight, but decisive, structural differences resolves a subtle size mismatch between Ba and Al still present in the Ae excess Laves phase "$Ba_7Al_{13}$". A similar situation was found for BaAlMg where the size mismatch between Ba and the B atom framework of the $MgNi_2$ structure resulted in an incommensurately modulated superstructure. BaAlMg, $Ba_{21}Al_{40}$, and related $Ba_{14}Al_{22+x}Zn_{5-x}$[28] beautifully demonstrate the structural and compositional flexibility of polar intermetallics to match size and electron count requirements for structural stability.

**Acknowledgment.** This work was supported by the Swedish Research Council (VR). One of the authors (T.Y.) is grateful for support from the Bio Nanotec Research Institute Inc., Japan.

**Supporting Information Available:** Crystallographic data in CIF format. Tables of lattice and atomic positional parameters, site occupancies, isotropic thermal parameters, and important interatomic distances. This material is available free of charge via the Internet at http://pubs.acs.org.

IC0400235